Soft Matter

Accepted Manuscript

ROYAL SOCIETY OF CHEMISTRY

www.rsc.org/softmatter

Journal Name

ARTICLE TYPE

Cite this: DOI: 10.1039/xxxxxxxxxx

Dewetting Transition Induced by Surfactant in Sessile Droplets at the Early Evaporation Stage

Xin Zhong,[a] and Fei Duan,[a,*]

Received Date
Accepted Date

DOI: 10.1039/xxxxxxxxxx

www.rsc.org/journalname

As surfactant is employed to control the wettability of solutions, we observe that the sessile droplet dewetting induced by autophobing exhibits a unique relation with the surfactant concentration. Below the critical micelle concentration (cmc) of the surfactant, the autophobic effect makes the droplet go through a rapid depinning at first (Phase 1) and then a relatively slower shrinkage (Phase 2). Unexpectedly, the rapid velocity of the three-phase contact line in Phase 1 shows a transition as the surfactant concentration increases above 0.043 cmc, while such transition is absent for the velocity in Phase 2. The spreading of the sessile droplets as they form before retraction, the maximum contact angle led by dewetting, and the droplet lifetime are as well regularly sensitive to the surfactant concentration. These phenomena are correlated with the assembling structure and the adsorbed amount at different interfaces with the loading of surfactant inventory.

1 Introduction

Wettability control of evaporating sessile droplets through the employment of surfactant can be realized simply and effectively based on the surface-active nature and the nonuniform distribution of surfactant at interfaces[1,2]. The role of surfactant in decreasing the surface energy at the liquid-air side[3–6], the reduction of the energy for liquid-air interfacial deformation[7], and the generation of Marangoni flow due to the spatially uneven distribution of surfactant[8,9] have been shown to vary the motion of the three-phase line and thus alter the deposition pattern if the droplet contains solutes[7,10,11]. The attempt to understand the phenomena is both scientifically interesting and technologically useful, particularly for the implications including inkjet printing[12,13], detergency[14], coating[15], bio-deposition[16], pesticide spraying[17] and oil recovery[1,18,19].

On the other side, the well-reported surfactant adsorption at the solid interface[18,20–22] which could lead to the autophobic effect, has received not as much attraction in terms of its influence in the dynamics of evaporating sessile droplet. Autophobing can be represented by the shrinkage of aqueous solutions in contact with the solid surface resulted from the reduction of surface energy by surfactant adsorption[23–25]. So far the broadly employed system for examining the autophobic effect is the Wilhelmy plate technique which requires a vertical solid plate to be inserted into a surfactant solution at a slow rate to induce a stick-slip-retreat behavior of the three-phase line. Limited by the weak mobility of the surfactant molecules across the bare solid surface, the autophobing was widely reported to be irrelevant to the surfactant concentration at a low value for such configuration[26]. For sessile droplets, however, the mechanisms responsible for the dependence of droplet dewetting on surfactant still remain debated, such as the critical concentration of surfactant for the cessation of autophobic effect and the correlation between the contact line retreat and the surfactant concentration[11,27–33]. Takenaka, et al.[33] demonstrated that the droplet dewetting exhibited a monotonous dependence on surfactant below the critical micelle concentration (cmc), while which is inconsistent with the findings of Frank and Garoff[26] that the contact line retreat is irrelevant to the surfactant inventory below 0.45 cmc. Motivated by these questions, we selected a wide range of surfactant concentration and experimentally investigated the autophobing-induced depinning of evaporating sessile droplet. For the first time we present that the retreat of the contact line displays a unique relation with the surfactant concentration. The shrinking velocity of the contact line for the initial rapid depinning phase shows a transition with an increase of the surfactant. Such transition, however, is unexpectedly absent for the subsequent slower depinning phase. Our finding of such relation between droplet depinning and surfactant might help the understanding of droplet wettability control with high application relevance.

2 Experimental Methods

We experimentally examined the effect of cationic surfactant on the spreading, the retraction and the evaporation of sessile

[a] School of Mechanical and Aerospace Engineering, Nanyang Technological University, 50 Nanyang Avenue, Singapore 639798, Singapore. E-mail: feiduan@ntu.edu.sg

droplets on silicon wafer substrates. Cetyltrimethylammonium bromide (CTAB; $C_{19}H_{42}BrN$, Sigma-Aldrich) was used as the surfactant to prepare solutions with concentration, C_{surf}, ranging from 0 mM to 1.4 mM. The critical micelle concentration (cmc) of the cationic CTAB is 0.92 mM[34]. We prepared the aqueous solutions by using nanofiltered water with a resistivity at 18.2 MΩ-cm, and the surfactant solutions were employed within 10 hours in avoidance of any decrease in surface activity[35]. The liquid-vapor surface tension, γ_{LV}, of CTAB-water solution was measured using the "pendent droplet" method with a consistent droplet volume at 2 μl by the tensiometer (Theta Optical Tensiometer, LTD2). The γ_{LV} value of the solutions, listed in Table 1, strongly agrees with the reported data[28,36]. Brand new silicon wafers (Latech Scientific Supply Pte. Ltd., hydrophilic) with the average roughness at 0.106 μm were thoroughly cleaned before each test. Controlled by a mechanical stage at a slow downward speed, the surfactant-water solution droplet was made gently touched with the horizontal substrate to minimize the effect of impingement. We evaluated the impact of the droplet by the Weber number, $We = \rho U^2 d/\gamma_{LV}$ in which ρ is liquid density, U is impact velocity, and d is droplet diameter. The downward speed of the mechanical stage was about 0.05 m/s while the initial wetted diameter of the droplet was roughly 3 mm. Based on the density and surface tension of pure water, the Weber number was calculated to be 0.06, almost two orders smaller than 1. Therefore, in our study the impact can be neglected and the initial droplet spread during placement was mainly driven by the capillary spreading mechanism. Once the droplet detached from the pipette tip, it spread to some extent to reach the maximum wetting area, and then retracted rapidly. In the following analysis, we set the moment at which the droplet stopped spreading at 0 s. Accordingly, we can measure the initial diameter, D_0, and the initial contact angle, θ_0. The dynamic evaporation of the droplet from a side view was investigated by the tensiometer equipped with a high-resolution digital camera at a frequency of 1 frame every second. The droplet volume at 2.75±0.14 μl used in the experiments was controlled by a micro-dosing system. The droplets were evaporating in an open condition with the pressure at 1 atm, the temperature at 23 ±1°C, and the relative humidity at 48±5%. The instantaneous contact angle, θ, the base diameter, D, and the droplet volume, V, were evaluated by the post-processing program, and the measurement accuracies were ±0.1°, ±0.1mm, and ±5%, respectively. The uncertainties of the post processing were evaluated within ±5%.

3 Results and Discussion

As the sessile droplets were made on the silicon substrate, the negatively charged silicon surface can attract the cationic heads of the surfactant molecules, and some of them assemble external to the contact line, leading to the reduction of the solid-vapor surface tension and dewetting of the droplet. Such autophobing-induced depinning behavior occurring at the initial stage of evaporation varies with the surfactant concentration, C_{surf}. Figure 1 shows the side view of the droplet by its images taken at 0 s and 40 s at intermediate C_{surf} to reveal the initial droplet behavior led by surfactant. The pure water droplet (Fig. 1 (a1)) with a small contact angle keeps pinning on the solid surface, and its contact angle decreases due to evaporation. The droplets with a lower range of C_{surf} from 0.014 mM to 0.6 mM (Fig. 1 (a2-a5)) autophobe intensively such that the contact angles increase and the base diameters decrease rapidly, while the one with a high C_{surf} at 0.84 mM (Fig. 1 (a6)) no longer retract but maintains pinning on the substrate from the very beginning.

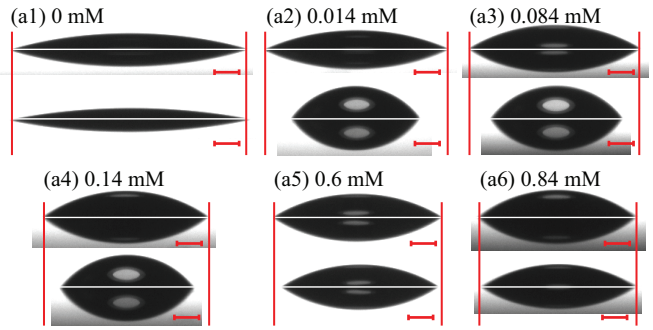

Fig. 1 The images at 0 s and 40 s for sessile droplets with the surfactant concentration, C_{surf}, at (a1) 0 mM, (a2) 0.014 mM, (a3) 0.084 mM, (a4) 0.14 mM, (a5) 0.6 mM, and (a6) 0.84 mM. The scale in the images indicates 0.5 mm.

To analyze the relation of the droplet dynamics and C_{surf}, we quantify the evolutions of the contact angle and the normalized base diameter over the full-spectrum of droplet lifetime. As shown in Fig. 2, the droplets with different C_{surf} exhibit varieties in the contact angle at t_0, the sudden depinning occurring mainly from 0 s to 100 s reflected by the increase of the contact angle and reduction of the base diameter, and the subsequent attenuated retraction till the end of drying. We mainly discuss the droplet dynamics at time t_0 and the initial depinning behavior later in this article. Once the initial depinning ceased, the droplets with C_{surf} below 0.084mM (0.09cmc) display the constant contact angle mode (CCA) and the mixed mode; as C_{surf} is above 0.084mM, only the mixed mode takes place; while for the one with C_{surf} higher than 0.84 mM (0.9cmc) the initial depinning is absent and the droplet maintains pinning on the solid surface at t_0. Therefore, the pinning effect is greatly enhanced by raising C_{surf} represented by the flattening trend of the normalized base diameter. The one with C_{surf} at 1.4 mM (about 1.5 cmc) shows a base diameter with invisible decrease except at the ultimate stage of drying.

The prominent stage of dewetting affected by surfactant concentration is from 0 s to approximately 100 s of the lifetime, during which the droplet evolves from the utmost spreading (0 s) to the initial depinning. The maximum spreading of the droplet before retraction is presented with D_0 in Fig. 3 (a) and θ_0 in Fig. 3 (b). The extent that the droplet utmost advances basically reduces with an increase in C_{surf}, presented by a shorter D_0 and a larger θ_0 at a higher C_{surf}. Marmur and Lelah[30] reported the similar results that the growing surfactant inventory suppressed the initial droplet spreading (circular symbols in Fig. 3 (a)). Although surfactant reduces the liquid-vapor surface tension, γ_{LV}, of the solutions (see Table 1) which reinforces the spreading, it is overwhelmed by the counteractive autophobic effect. As the

Table 1 The value of the liquid-vapor surface tension, γ_{LV}, at the listed surfactant concentration, C_{surf}.

C_{surf} (mM)	0.014	0.028	0.042	0.06	0.084	0.14	0.28	0.42	0.84
γ_{LV} (mN/m)	69.6	68.5	68.4	68.4	66.3	64.2	58.1	53.2	40.5

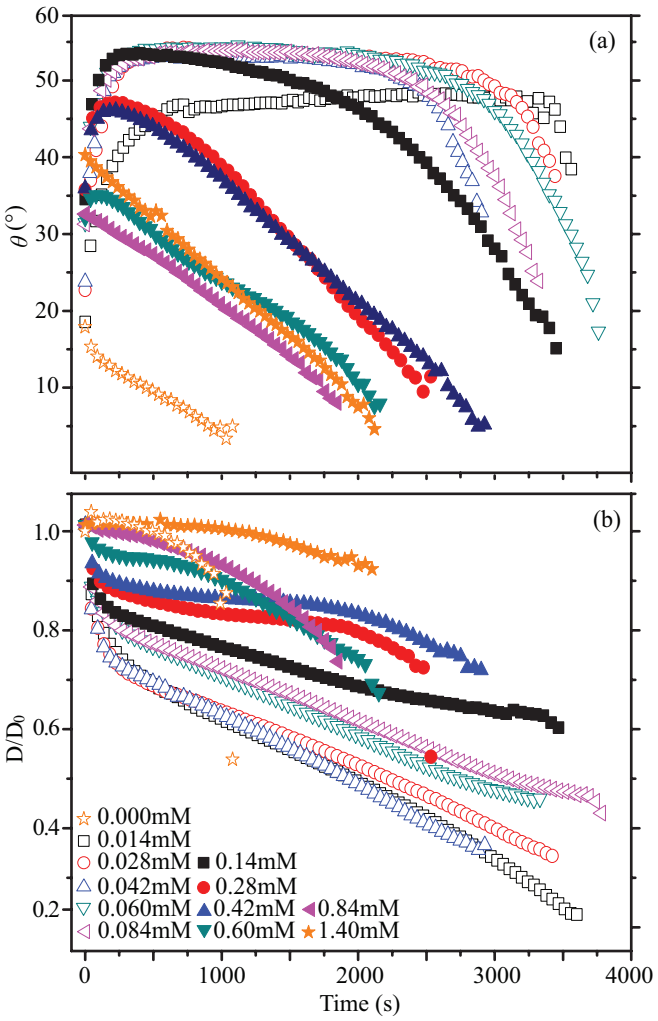

Fig. 2 (a) Contact angle, θ, and (b) the normalized base diameter, D/D_0, as a function of time for the sessile droplets with different surfactant concentrations.

droplet is made on the silicon wafer, some surfactant molecules in the thinning front transport across the contact line and locate at the bare solid-vapor interface to form a hydrophobic barrier. When the barrier is sufficiently built up it can halt the contact line motion immediately. Indeed, increasing C_{surf} can facilitate the establishment of such a hydrophobic barrier. The area covered by surfactant at the bare solid-vapor interface was proportional to C_{surf} as reported by Frank and Garoff[31,32]. Therefore, any further spreading of the droplet can be terminated responsively with an increasingly effective arrival of the surfactant beyond the contact line.

The sufficiently established hydrophobic barrier halts the spreading, and meanwhile initiates the contact line depinning abruptly. We observed that such depinning stage displays two distinct phases: at first the contact line retreats rapidly for less than several seconds, and then the velocity abruptly reduces and sustains to about 100 s. Therefore, we divide the depinning stage into Phase 1 featuring quick retreating and Phase 2 of slower shrinkage. After that the droplet contact line moves even slower till the droplet dries out. The evolution of the base diameter for the first 100 s featuring intense depinning is shown in Fig. 4 (a). Through directly differentiating the base radius with time, we obtained the instantaneous retreat velocity, U, of the contact line at various C_{surf} (Fig. 4 (b)). U falls sharply during the first several seconds, and then its declining trend slows down and towards flattening with small oscillations over a longer period. We plot the best-fitting line in the inset of Fig. 4 (b) as an example to determine the cut-off point for Phases 1 and 2. The average velocity with the reference to $D_0/2$ for Phase 1 and Phase 2 are denoted by $\bar{U}_1$ and $\bar{U}_2$. As shown in Fig. 5 (a,b), $\bar{U}_1$ is one order of magnitude higher than that of $\bar{U}_2$. Besides, the trend of $\bar{U}_1$ and $\bar{U}_2$ are surprisingly inconsistent with the increase of C_{surf}. They suggest that either the mechanisms controlling the contact line motion or the relative weight for each mechanism alters from Phase 1 to Phase 2.

In respect to Phase 1, $\bar{U}_1$ rises first and then declines with the increase of C_{surf}. The velocity apex falls at around 0.042 mM (0.043 cmc), which is near the point of zero charge (p.z.c.=0.05 cmc)[27]. On the basis of Young's equation, as the droplet is out of equilibrium, the tension, f, acting at the contact line and driving it into motion can be expressed as

$$f = \gamma_{LV} cos\theta + \gamma_{SL} - \gamma_{SV}, \quad (1)$$

where γ_{SL} and γ_{SV} are the solid-liquid and the solid-vapor surface tensions, and θ is the dynamic contact angle. The transition of $\bar{U}_1$ is attributed to the combined results of the surfactant-dependent surface tensions at the three interfaces. Below p.z.c., γ_{LV} (Table 1) remains relatively stable against the increase of C_{surf}. At the solid-liquid interface, as the adsorption is in the form of monomers (the left schematics of the inset of Fig. 5 (a)) obeying the two-step adsorption model[34], the adsorbed amount shows nuance with an increase of the surfactant and thus the resulted γ_{SL} remains nearly invariable. But since a higher C_{surf} enhances the amount of surfactant arriving at the bare solid-vapor interface beyond the contact line (the left schematics of the inset of Fig. 5 (a)) and thus the reduction of γ_{SV}[31], it dominates and reinforces the inward motion.

Above the p.z.c., the monomers at the solid-liquid interface have reached saturation. Surfactant molecules in the bulk start to assemble with the monomers to form admicelles (the right schematics of the inset of Fig. 5 (a)). It can lead to a roughly ten-folded adsorbed amount particularly when approach the cmc and thus a substantial decrease of γ_{SL}[27]. The synergetic reductions of γ_{SL} and γ_{LV} (Table 1) compete and eventually overwhelm the decrease of γ_{SV}, thus the increase of the inward velocity

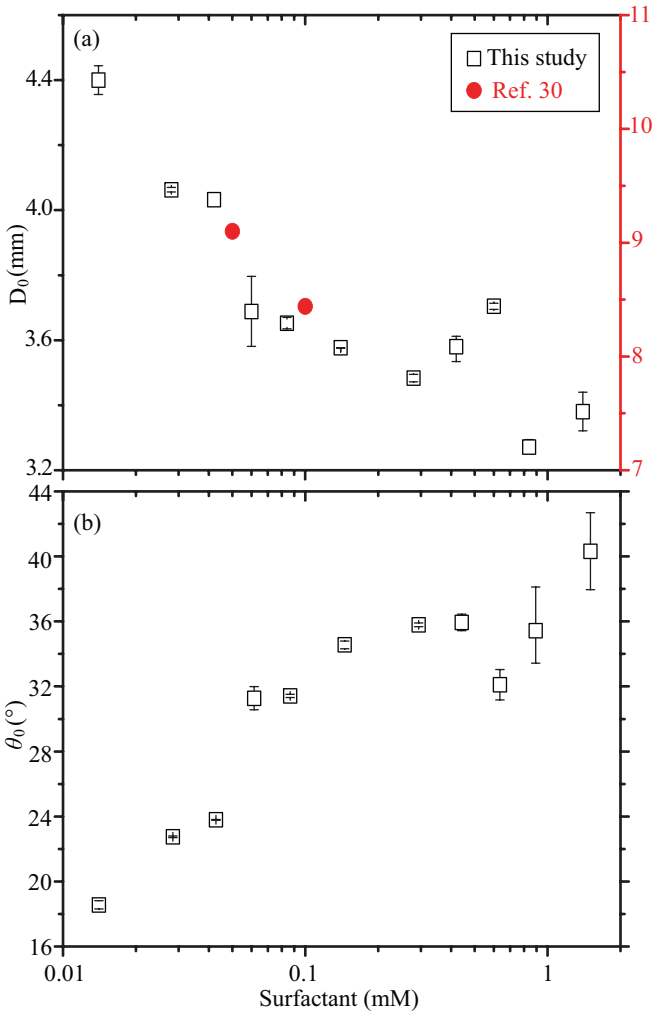

Fig. 3 (a) The initial base diameter, D_0, in this study and from Ref. 30 as a function of C_{surf}. (b) The change of the initial contact angle, θ_0, with C_{surf}.

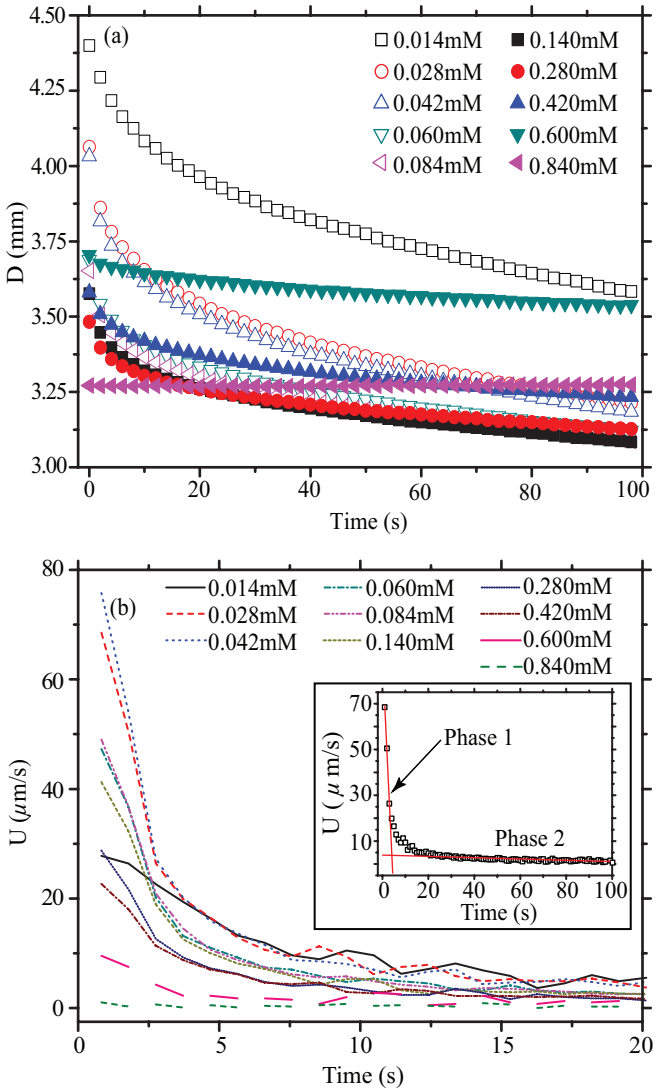

Fig. 4 (a) Base diameter, D, versus time for the initial 100 s. (b) The retreat velocity, U, of the contact line versus time for the initial 20 s at surfactant concentrations. The inset in (b) is an example to show the transition from Phase 1 to Phase 2 from the best linear fitting.

$\bar{U}_1$ is terminated and turned into downwards. Besides, $\bar{U}_1$ has been examined as well for the CTAB droplets[30] and the HTAB (Hexadecyltrimethylammonium bromide) droplets on glass slides[33] (Fig. 5 (a)). The velocity for either CTAB or HTAB on glasses increased monotonously with C_{surf} and no transition emerged. It may be attributed to the different property of glass slide or the smaller range of C_{surf}.

As illustrated in Fig. 5 (b), such transition in $\bar{U}_1$ does not show up for $\bar{U}_2$ which decreases monotonously with an increase of C_{surf}. It implies that the comprehensive effects of surface tensions at the three interfaces varied by surfactant adsorption cannot afford an increase of $\bar{U}_2$ below the p.z.c. Unlike the bare solid-vapor interface in Phase 1, Phase 2 has the solid-vapor interface used to be covered by the solution and it is formed through the withdrawal motion of the contact line, as depicted by the arrows in the inset of Fig. 5 (b). Surfactant on such surface has a "standing up" structure while the counterparts for Phase 1 are "lying down" assemblies[31,37]. The sensitivity of the two types of structures to C_{surf} should be different and thus leads to different degrees of reduction in γ_{SV}. Additionally, with C_{surf} lower than the p.z.c., we notice that the dynamic contact angle, θ, is larger at a higher C_{surf} at a same moment. The resulted smaller horizontal component of γ_{LV}, $\gamma_{LV}\cos\theta$, possibly accounts for the unidirectional decrease of $\bar{U}_2$.

The entire retraction of the droplet can be controlled either by autophobing, evaporation, or both[11]. The role of each mechanism can be evaluated by comparing their characteristic time scales as reported by Qu, et al.[37]. The duration of the unsteadiness of the moving contact line is on the inertial time scale and is described as $t_i = \rho L^2/\mu$, in which ρ is the solution density, L is the capillary length, and μ is the viscosity. In the vicinity of the contact line, the evaporation time scale can be expressed as $t_e = L\mu\rho/(\gamma_{LV}\rho_v)$, in which ρ_v is the vapor density. In our experiments, t_i ranges from 4 to 7 s, and t_e is approximately 1 s. The unsteadiness, t_i, is highly compatible with the duration of Phase 1 for the surfactant solution droplets. The time scale of evaporation, t_e, suggests that the evaporation reached stability

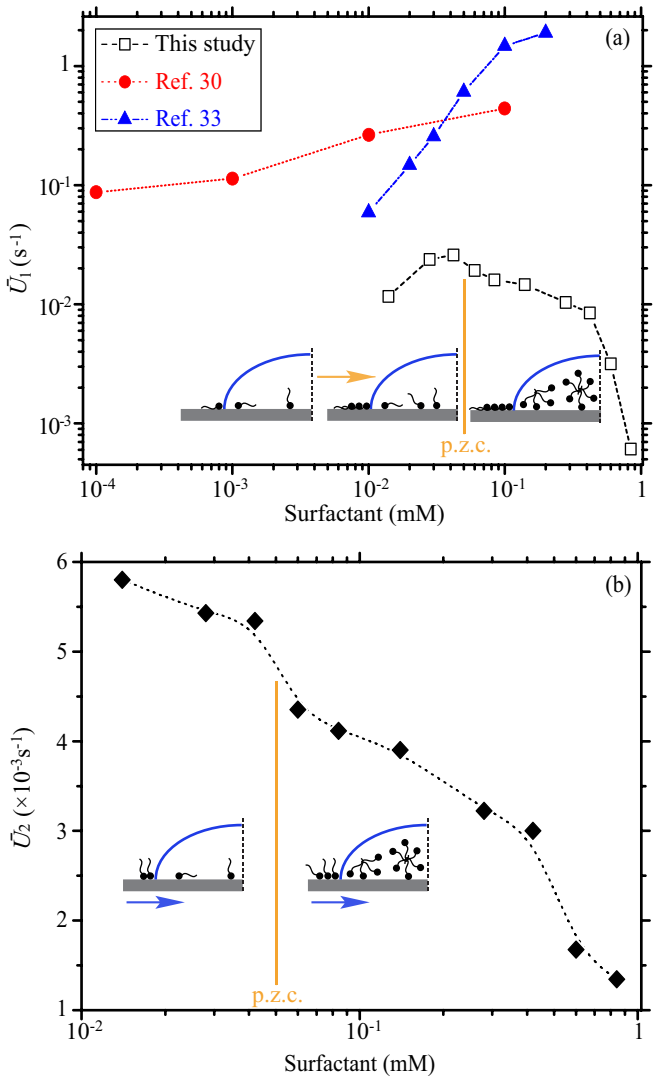

Fig. 5 The averaged velocity $\bar{U}_1$ in Phase 1 ar a function of C_{surf} in this study and from Refs. 30, 33. The inset is $\bar{U}_2$ in Phase 2 of early evaporation stage.

within around 1 s, coincident with the linear reduction of the droplet volume over time. The withdrawal velocity of the contact line solely driven by evaporation can be estimated under the CCA mode from the measured average evaporation rate and the initial base diameter at each C_{surf}. The evaporation induced contact line velocity is around 0.1 μm/s, agreeing with the study of Qu, et al.[37]. We found that the evaporation-driven contact line motion is approximately 2 orders and 1 order of magnitude lower than $\bar{U}_1$ and $\bar{U}_2$, respectively. Therefore, the autophobic effect dominated the initial rapid retraction and it very likely controlled the second phase as well.

By the end of the initial depinning the droplet entered either the CCA or the mixed mode. No matter in which mode the maximum contact angle, θ_{max}. was reached. Figure 6 (a) illustrates θ_{max} as a function of C_{surf}. θ_{max} rises first and then falls, leaving its apex at 0.084 mM of C_{surf}. By assuming that the droplet with θ_{max} has almost approached the equilibrium, the wetting tension at θ_{max}, denoted by τ_{max}, can be expressed with $\gamma_{LV} cos\theta_{max}$. Therefore, τ_{max} exhibits an opposite trend as compared to θ_{max} (Fig. 6 (b)). The transition in θ_{max} and τ_{max} implies that the dominant mechanism for them should be the same for $\bar{U}_1$.

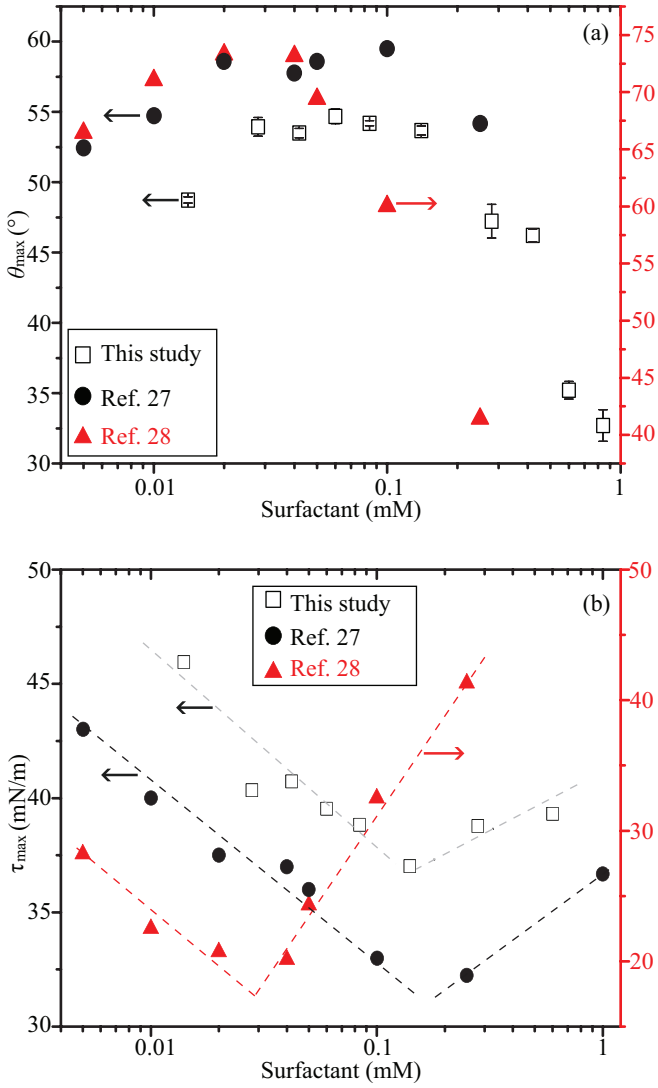

Fig. 6 (a) The maximum contact angle, θ_{max}, as a function of surfactant concentration, C_{surf} in the study and from Refs. 27, 28. (b) The wetting tension, τ_{max}, with the surfactant concentration, C_{surf}, in this study and for Refs. 27, 28.

It is worthy noticing that the transition point of θ_{max} is delayed to 0.06 mM as compared to 0.042 mM for $\bar{U}_1$. The inward tension, f, at t_0 in Phase 1 is partially determined by the initial contact angle, θ_0, which positively depends on C_{surf}. Therefore, the horizontal component of γ_{LV} at t_0 is smaller at a higher C_{surf}. Thus the upward trend of $\bar{U}_1$ can be terminated more responsively and then turned to downwards as C_{surf} increases over the p.z.c. We compare our results with those from Refs. 27, 28 in Fig. 6 (a,b). The system employed in Ref. 27 was a vertical silica plate partly immersed in a CTAB solution, and the other in Ref. 28 was a sessile droplet on a horizontal mica plate. In Ref. 27, as the plate was forced into the solution, the contact line exhibited a stick-jump and then an autophobic behavior. For both systems the

results exhibited resemblance to the ones for our study. But for the mica surface the trends of θ_{max} and τ_{max} shift leftwards than the ones for the silica and silicon surfaces, which are possibly resulted from a variation of surface tension with C_{surf}. The larger equilibrium contact angle implies a more intense autophobing of the droplet on mica than on the silica or silicon surface.

4 Conclusion

In summary, we presented systematic experimental results that the depinning of a sessile droplet due to autophobing varied non-monotonously with the surfactant concentration. We primarily examined the utmost spreading of the droplet, the contact line motion showing two distinct phases during the initial depinning stage, and the maximum dewetting that the droplet could reach. A transition emerged in the averaged velocity for the rapid depinning phase, while such transition was disappeared in the subsequent slower depinning phase. The transition manifested as well in the maximum contact angle with a higher loading of surfactant. The unique relation between the droplet shrinkage and surfactant concentration could improve the understanding of autophobing in wettability control of droplet and promote its intersection with the emerging field of the colloidal droplet evaporation. It is still a challenging work for quantifying and visualizing local surfactant at the interfaces of the evaporating droplet at the initial depinning stage as the contact line moves, however, further study would greatly enrich the knowledge of the relation between contact line dynamics and surfactant adsorption.

Acknowledgements

The authors acknowledge the support of MOE AcRF Tier 1 (RG120/14).

References

1 D. K. Sinz, M. Hanyak and A. A. Darhuber, *The Journal of Physical Chemistry Letters*, 2013, **4**, 1039–1043.
2 X. Zhong, A. Crivoi and F. Duan, *Advances in colloid and interface science*, 2015, **217**, 13–30.
3 S. Semenov, A. Trybala, H. Agogo, N. Kovalchuk, F. Ortega, R. G. Rubio, V. M. Starov and M. G. Velarde, *Langmuir*, 2013, **29**, 10028–10036.
4 K. Sefiane, *Journal of Petroleum Science and Engineering*, 2006, **51**, 238–252.
5 O. Soboleva and B. Summ, *Colloid Journal*, 2003, **65**, 89–93.
6 S. J. Gokhale, J. L. Plawsky and P. C. Wayner, *Langmuir*, 2005, **21**, 8188–8197.
7 P. J. Yunker, T. Still, M. A. Lohr and A. Yodh, *Nature*, 2011, **476**, 308–311.
8 T. Still, P. J. Yunker and A. G. Yodh, *Langmuir*, 2012, **28**, 4984–4988.
9 T. Kajiya, W. Kobayashi, T. Okuzono and M. Doi, *The Journal of Physical Chemistry B*, 2009, **113**, 15460–15466.
10 A. Crivoi and F. Duan, *The Journal of Physical Chemistry B*, 2013, **117**, 5932–5938.
11 X. Zhong and F. Duan, *Langmuir*, 2015, **31**, 5291–5298.
12 L. Zhang, H. Liu, Y. Zhao, X. Sun, Y. Wen, Y. Guo, X. Gao, C.-a. Di, G. Yu and Y. Liu, *Advanced Materials*, 2012, **24**, 436–440.
13 M. Hanyak, A. A. Darhuber and M. Ren, *Journal of Applied Physics*, 2011, **109**, 074905.
14 G. Cutler, *Detergency: theory and technology*, CRC Press, 1986, vol. 20.
15 H. Uchiyama, D. Shimaoka and H. Kozuka, *Soft Matter*, 2012, **8**, 11318–11322.
16 A. T. Woolley and R. T. Kelly, *Nano Letters*, 2001, **1**, 345–348.
17 D. T. Wasan, M. E. Ginn, D. O. Shah *et al.*, *Surfactants in chemical/process engineering*, M. Dekker, 1988.
18 F. Mugele, B. Bera, A. Cavalli, I. Siretanu, A. Maestro, M. Duits, M. Cohen-Stuart, D. van den Ende, I. Stocker and I. Collins, *Scientific reports*, 2015, **5**, 10519.
19 P. A. Ash, C. D. Bain and H. Matsubara, *Current Opinion in Colloid & Interface Science*, 2012, **17**, 196–204.
20 R. E. Lamont and W. A. Ducker, *Journal of the American Chemical Society*, 1998, **120**, 7602–7607.
21 H. Fan, Y. Lu, A. Stump, S. T. Reed, T. Baer, R. Schunk, V. Perez-Luna, G. P. Lopez and C. J. Brinker, *Nature*, 2000, **405**, 56–60.
22 D. Sun, A. E. Riley, A. J. Cadby, E. K. Richman, S. D. Korlann and S. H. Tolbert, *Nature*, 2006, **441**, 1126–1130.
23 W. A. Zisman, *Adv. Chem.*, 1964, **43**, 1–51.
24 E. Hare and W. Zisman, *The Journal of Physical Chemistry*, 1955, **59**, 335–340.
25 H. Fox, E. Hare and W. Zisman, *Journal of Colloid Science*, 1953, **8**, 194–203.
26 B. Frank and S. Garoff, *Colloids and Surfaces A: Physicochemical and Engineering Aspects*, 1996, **116**, 31–42.
27 V. Yaminsky and K. Yaminskaya, *Langmuir*, 1995, **11**, 936–941.
28 L. T. Eriksson, P. M. Claesson, J. C. Eriksson and V. V. Yaminsky, *Journal of colloid and interface science*, 1996, **181**, 476–489.
29 V. Yaminsky, B. Ninham and M. Karaman, *Langmuir*, 1997, **13**, 5979–5990.
30 A. Marmur and M. D. Lelah, *Chemical Engineering Communications*, 1981, **13**, 133–143.
31 B. Frank and S. Garoff, *Langmuir*, 1995, **11**, 4333–4340.
32 B. Frank and S. Garoff, *Langmuir*, 1995, **11**, 87–93.
33 Y. Takenaka, Y. Sumino and T. Ohzono, *Soft matter*, 2014, **10**, 5597–5602.
34 E. Tyrode, M. W. Rutland and C. D. Bain, *Journal of the American Chemical Society*, 2008, **130**, 17434–17445.
35 E. J. Burcik and C. R. Vaughn, *Journal of Colloid Science*, 1951, **6**, 522–527.
36 N. M. van Os, J. R. Haak and L. A. M. Rupert, *Physico-chemical properties of selected anionic, cationic and nonionic surfactants*, Elsevier, 2012.
37 D. Qu, R. Suter and S. Garoff, *Langmuir*, 2002, **18**, 1649–1654.